COMMUNICATION

Solvent-Vapor-Induced Tunability of Self-Assembled Block Copolymer Patterns

By *Yeon Sik Jung*, and *Caroline A. Ross**

Well-controlled monolayer patterns of microdomains of block copolymers (BCPs) have been widely pursued for applications in sub-30-nm nanolithography.[1–11] BCP film processing is scalable and low cost, and is compatible with existing semiconductor fabrication techniques. Di-BCP with a molecular weight of a few tens to a few hundreds of $kg\,mol^{-1}$ have been known to spontaneously form periodic arrays of well-defined nanoscale features, such as dots, holes and lines, which have been used as masks in the fabrication of arrays of nanoscale functional features after the selective elimination of one block.[1–3,11] Long-range ordering and positional registration of the features has been imposed by using chemical or topographical templates.[3,4,12,13] The morphology of the patterns has been further diversified by using multi-BCPs or employing various confinement geometries.[6,14–16] The morphology and length scale of the microdomain arrays of BCPs are governed by the degree of polymerization of each block,[17,18] and thus to obtain different geometries and feature sizes, polymers with different chain lengths or BCP–homopolymer blends have been employed.[19] However, in terms of device fabrication, it would be advantageous to be able to manipulate the shape and dimensions of features composed of a single BCP by simply altering the processing conditions.

Polymeric materials often provide an exceptional degree of controllability in their molecular configurations due to their weak intermolecular forces, which are largely based on Van der Waals interactions. Solvent vapor annealing, which has been employed to increase chain flexibility in BCPs and to promote their self-assembly into the microphase-separated state,[11,20–26] may be used as an effective lever to engineer the resulting structures. It has been shown that treatments with selective or nonselective vapor result in different morphologies or orientations, demonstrating solvent-induced controllability.[26–28] However, precise adjustment of pattern size and morphology using controlled mixed solvent vapors has not been studied to the best of our knowledge.

In this Communication, we report on the systematic tunability of the dimensions and morphology of patterns of microphase-separated BCP; this was achieved by controlling the solvent-annealing conditions, where the key parameters are solvent vapor pressure and the mixing ratio of selective and partially selective solvent vapors. Vapor pressure can control the degree of solvent uptake by the film, which changes both the chain mobility and the interfacial interaction between the blocks of the BCP. We will also propose the theoretical model explaining the increasing size of the pattern period with decreasing vapor pressure. It has been recently reported that a change in the effective volume fraction of the blocks can be accomplished using selective and nonselective vapors.[26,27] We will show independent control of pattern size and periodicity by using a mixed vapor containing selective (heptane) and partially selective (toluene) solvents. We will also demonstrate that a cylinder-forming BCP can be transformed into a perforated lamellar structure by increasing the portion of selective solvent in the mixed vapor. This study suggests a way to relieve the constraints, imposed by the molecular structure of BCPs, on the achievable microdomain geometries.

We have previously presented high quality nanoscale lines, dots and rings composed of a poly(styrene-*b*-dimethylsiloxane) (PS–PDMS) di-BCP.[11,16,29] This polymer is useful for nanolithography in that its self-assembled microdomain pattern has a large correlation length that can exceed several micrometers and a low defect density, even in the absence of templating. High etch selectivity between its two blocks is also possible due to the existence of Si in the PDMS backbone. As described in Figure 1a, a PS-PDMS BCP with a molecular weight of $45.5\,kg\,mol^{-1}$ and 33.5 vol% PDMS was spin-coated onto a Si substrate and solvent-annealed forming a PS matrix containing a monolayer of PDMS cylinders that were parallel to the substrate. There was also a PDMS layer at the interfaces of the BCP with the substrate and air due to its lower surface energy compared to PS.[11] Etching away the surface layer of PDMS and some of the PS matrix revealed the arrangement of the now-oxidized PDMS cylinders.[11,16,29]

We consider first the effect of solvent vapor pressure on the morphology of the cylinder patterns. The vapor pressure is characterized by the ratio between S, the surface area of the solvent while in a beaker placed within the solvent-annealing chamber, and V, the volume of air that will mix with the solvent vapor, which is equivalent to the amount of air in the chamber at atmospheric pressure. The chamber had a small leak path through which solvent vapor could escape. The amount of solvent vapor in the chamber was determined by three flux components: evaporation from the solvent surface (F_1), condensation onto the solvent surface (F_2), and leak flow (F_3). At steady state, the concentration (C) of the solvent vapor in the chamber is given by

$$C = \frac{a_0(F_1 - F_2 - F_3)}{V} = \frac{a_1 S - a_2 S \cdot C - a_3 \cdot C}{V} = \frac{a_1 S}{a_2 S + a_3 + V} \quad (1)$$

[*] Prof. C. A. Ross, Y. S. Jung
Department of Materials Science and Engineering
Massachusetts Institute of Technology
Cambridge, Massachusetts 02139 (USA)
E-mail: caross@mit.edu

DOI: 10.1002/adma.200802855

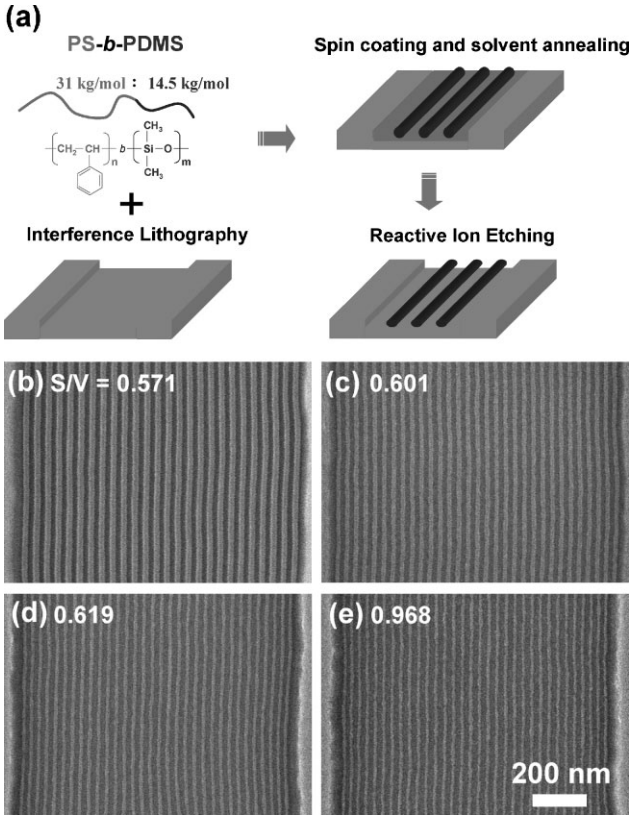

Figure 1. a) Schematic of processing steps used to obtain PS–PDMS BCP microdomains. The cylinder-forming PS–PDMS BCP was spin-coated on topographically patterned substrates, solvent-annealed with mixed solvent vapors, and treated with CF_4 and O_2 plasmas. The PDMS layers at the substrate/BCP and air/BCP interfaces are not shown. b–e) SEM images of the cylinder-forming PS–PDMS BCP after solvent-annealing and reactive-ion etching to remove the PS matrix. Linear patterns with various periodicity and linewidths were obtained by using different toluene vapor pressure conditions. The solvent vapor pressure was varied by changing the ratio of the solvent surface area (S) to the annealing chamber volume (V). The S/V ratios are 0.571 (b), 0.601 (c), 0.619 (d), and 0.968 (e) cm^{-1}.

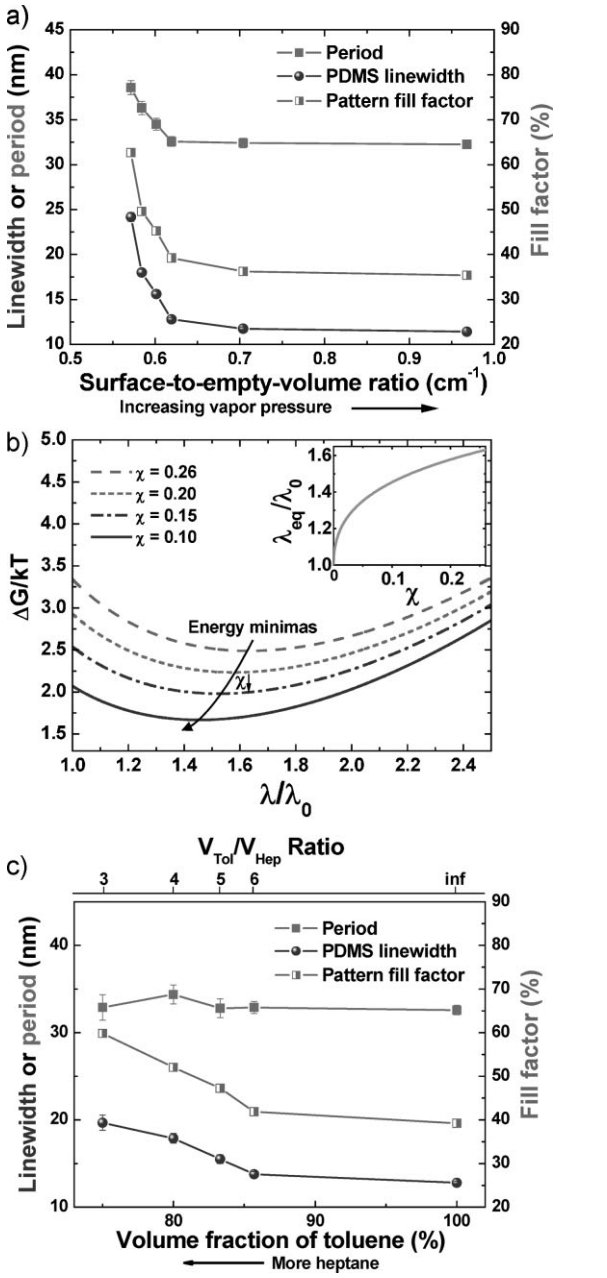

Figure 2. a) Period length, linewidth, and fill factor of each pattern as a function of S/V. b) Calculated free energy curves with different χ parameters. The inset shows the change of equilibrium domain spacing with χ. c) Period length, linewidth, and fill factor of each pattern obtained using different mixing ratios of toluene and heptane. The volume fraction of toluene was calculated as $V_{Tol}/(V_{Tol}+V_{Hep})$.

where $a_{i=0,1,2,3}$ are proportionality constants. Equation 1 shows that there is an inverse proportionality between the vapor pressure (or the concentration, C) and the air volume. Thus, to identify the effects of vapor pressure on morphology, S was fixed at 5.16 cm^2 while V was changed from 5.3 to 9.0 cm^3 in our experiments.

Figure 1b–e presents scanning electron microscopy (SEM) images of oxidized PDMS patterns as a function of S/V while Figure 2a shows changes in period length, linewidth (cylinder diameter), and fill factor (linewidth/period length). The PS–PDMS was templated by shallow grooves in the Si substrate, forming cylinders in well-ordered parallel arrays. Only 20 patterns within the central region of each trench were used for analysis since template edges may affect the height profile of polymer films and reduce the length of the pattern period, as reported previously.[3] The length of the pattern period decreased from 38.6 to 32.3 nm, a change of 19.5%, as the vapor pressure increased from 0.57 to 0.97 cm^{-1}, and the linewidth decreased by 112% from 24.2 to 11.4 nm. The majority of the changes occurred within the lower vapor-pressure regime ($S/V = 0.57$–$0.70\ cm^{-1}$). Changes in pattern dimensions were consistent with previous reports, in which domain spacing varied with vapor pressure[30] and the concentration of polymer in solution.[31] Due to the screening effect of the solvent molecules, the effective Flory-Huggins interaction parameter (χ_{eff}) decreases as the volume

fraction (f_s) of solvent in the film increases:[18,31]

$$\chi_{eff} = \chi(1 - f_s) \quad (2)$$

where χ is the interaction parameter in the absence of solvent uptake. Consequently, solvent uptake in BCP films decreases the effective segregation strength, $\chi_{eff}N$, where N is the degree of polymerization, and thus affects the equilibrium domain spacing.

The Gibbs free energy change (ΔG) with respect to a reference state can be expressed as a function of domain spacing (λ) by assuming that the total free energy per polymer chain is the sum of the interfacial energy and the chain conformational energy.[16,29,32–34] The reference state, where the free energy is zero, consists of relaxed homopolymers without interfaces between the two polymer blocks. The derivation of the free energy expression is described in the Supporting Information, and leads to

$$\Delta G(\lambda) = \frac{kT}{a^2}\sqrt{\frac{\chi_{eff}}{6}} \cdot 2Ma^3 \cdot \frac{1}{\lambda} + \frac{1}{2}kT \cdot \left[\frac{\lambda^2}{4Ma^2} + \frac{4\sqrt{Ma^2}}{\lambda} - 3\right] \quad (3)$$

where k, T, a, M, and Σ denote the Boltzmann constant, the temperature, the Kuhn step size, the total number of Kuhn segments, and the contact area per chain between the two blocks, respectively. When χ is zero, the chains are fully relaxed exhibiting maximum conformational entropy, and λ is equivalent to $\lambda_0 = 2aM^{1/2}$, which is twice the end-to-end distance of a Gaussian chain since one period is composed of two polymer chains. As χ increases, the conformational structure becomes more perturbed and λ increases. The equilibrium domain spacing (λ_{eq}) can be determined by differentiating Equation 3 with respect to λ and equating it to zero. In the strong segregation limit (high χ), the chains would be stretched 10–40% by microphase separation compared to those in the relaxed state due to the unfavorable contacts between different blocks;[35,36] the $1/\lambda$ component of the strain energy term would be small, and λ_{eq} would be approximately equivalent to $a\chi^{1/6}N^{2/3}$. Figure 2b shows the shift of the minimum in the free energy curves towards larger domain spacing as χ is increased, and the inset presents the calculated dependence of λ_{eq} on χ. By increasing the domain spacing and thus, decreasing the interfacial area per chain, at higher χ, the interfacial energy can be reduced at the expense of increased strain energy (stemming from decreased conformational entropy). This free energy model explains the decrease of period length in the pattern as the solvent vapor pressure is increased during annealing.

Figure 2a also shows that the pattern fill factor decreased from 62.7 to 35.4% as S/V increased from 0.57 to 0.97 cm^{-1}, which indicates that the PDMS linewidth decreased faster than the period length with increasing S/V. This may be attributed to the fact that toluene is a partially selective solvent for the PS block. Although PDMS also dissolves well in toluene, it has a larger solubility parameter difference with toluene ($|\delta_{Tol} - \delta_{PDMS}| = |18.2–15.5| = 2.7\ MPa^{1/2}$) than PS does ($|\delta_{Tol} - \delta_{PS}| = |18.2–18.5| = 0.3\ MPa^{1/2}$).[37] Thus, we expect that toluene leads to a higher degree of swelling in PS than in PDMS. It should also be noted that the density of defects, such as Y junctions, increased as the vapor pressure decreased due to reduced chain mobility.

While the results in Figure 1b–e and 2a demonstrate the ability of this technique in manipulating period length and linewidth, the two dimensions cannot be varied independently. We devised a method using mixed solvent to understand their correlation with one another. Heptane ($\delta_{Hep} = 15.3\ MPa^{1/2}$) is a good solvent for PDMS, but a poor solvent for PS.[37] The measurements in Figure 2c and corresponding SEM images in Figure 3a–b show the variations of period length, linewidth, and fill factor with the ratio of volume of liquid toluene to liquid heptane (V_{Tol}/V_{Hep}) at $S/V = 0.62\ cm^{-1}$ in the chamber. For $V_{Tol}/V_{Hep} > 3$, PDMS formed parallel cylinders with little variation in period length, but with a systematic change in linewidth and fill factor. The increase of linewidth with the increasing fraction of heptane in the vapor (decreasing V_{Tol}/V_{Hep}) was a result of the selective increase of the effective volume fraction of PDMS by heptane. The very small variation in pattern periodicity may be explained by the fact that the PS domains shrank as PDMS domains expanded. As a result, an increase in the volume fraction of heptane from 0 to 25% led to

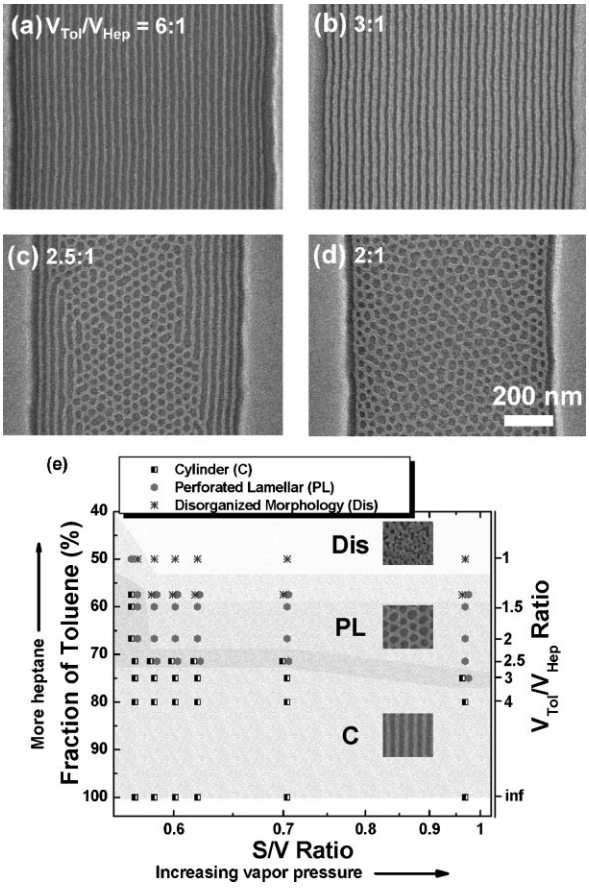

Figure 3. a–d) SEM images of films showing the evolution of morphology as V_{Tol}/V_{Hep} is varied: 6 (a), 3 (b), 2.5 (c), and 2 (d). e) Phase diagram indicating morphology obtained at various solvent mixing ratios and vapor pressures. A complete perforated lamellar structure was obtained at $V_{Tol}/V_{Hep} = 2$.

a 54% linewidth increase, from 12.8 to 19.7 nm, without an appreciable change in period length. A larger defect density was also observed with a higher heptane fraction, and the trend likely arises from the decreased chain mobility of the majority PS block. These results suggest a convenient way to fabricate line patterns with a desired period length and linewidth. First, an appropriate vapor pressure condition can be determined for the chosen period length; a specific linewidth can then be obtained by treating the polymer film with vapor having the proper toluene/heptane ratio.

The morphology undergoes a striking change as the fraction of heptane increases further ($V_{Tol}/V_{Hep} < 3$). Figure 3c–d and S1 (see Supporting Information) present the evolution of the PDMS domain geometry from cylinders to perforated lamellae, and eventually to a disorganized morphology, as the fraction of heptane (and consequently the effective volume fraction of PDMS) increases. Hexagonally perforated lamellar phases, where the minority block forms a lamella with holes arranged in sixfold symmetry, have been reported for BCPs with a volume fraction range between those corresponding to cylindrical and lamellar phases; examples include poly(styrene-*b*-butadiene-*b*-styrene) and poly(styrene-*b*-2-vinylpyridine-*b*-t-butyl methacrylate), which are both tri-BCP thin films, and poly(styrene-*b*-methyl methacrylate), a di-BCP thin film.[30,38,39] It has also been reported that a transition from lamellae to perforated lamellae can be induced by selectively swelling a polyethylene oxide block in a poly(ethylene oxide-*b*-methyl methacrylate-*b*-styrene) tri-BCP film.[27] The poor etch-selectivity or the formation of multiple lamellae in these examples, however, made them less useful for lithographic applications.

The mixed morphology of cylinders and perforated lamellae seen at $V_{Tol}/V_{Hep} = 2.5$ (Fig. 3c) suggests the possibility of forming mixed morphologies controllably in a single annealing step. It is likely that the shallow steps in the substrate stabilized the parallel cylinders, while the perforated lamella formed at the center of the substrate trench. The most uniform perforated lamellar structure was obtained at $V_{Tol}/V_{Hep} = 2$ (Fig. 3d). At higher heptane ratios ($V_{Tol}/V_{Hep} < 1.5$), the size and spacing of the perforations increased and the structure became disorganized (Fig. S1). Further studies using a variety of solvents may arise in additional ways to tune the microphase-separated structures.

The different morphologies obtained using various V_{Tol}/V_{Hep} and S/V ratios are presented as a phase diagram in Figure 3e. As expected, the dominant factor controlling the morphology was the solvent ratio. For every S/V ratio, the morphology similarly evolved from cylinders, through perforated lamellae, to a disorganized structure (Fig. 3 and S1). However, the morphology was also influenced slightly by vapor pressure. At the lowest vapor pressure condition ($S/V = 0.53\,cm^{-1}$), cylindrical morphologies were observed even with relatively high heptane fraction, but at higher S/V values perforated lamellar or poorly ordered morphologies occurred at a lower heptane fraction. These results suggest that a higher vapor pressure at a fixed V_{Tol}/V_{Hep} ratio would slightly increase the effective volume fraction of PDMS. This can be explained by the partial selectivity of toluene and the selectivity of heptane. In general, the majority of toluene molecules interact with PS due to a small energy penalty. However, as the degree of PS swelling increases, an entropic effect resulting from the stretching may drive more toluene molecules into the PDMS block and therefore make toluene a less selective solvent, which is consistent with the saturated fill factor at high vapor pressure ($S/V > 0.7$), shown in Figure 2a. On the other hand, the highly selective nature of heptane enhances the effective volume fraction of PDMS as the vapor pressure increases, leading to an increase in line width.

The influence of vapor pressure on the ordering of the perforated lamellar structure was investigated at a fixed solvent ratio of $V_{Tol}/V_{Hep} = 2$. Figure 4a–d and S2a-b (see Supporting Information) demonstrate the change in the degree of order of the perforations depending on the vapor pressure. The ordering can be improved by lowering the vapor pressure, which is attributed to a larger χ_{eff} and consequently a higher thermodynamic driving force for microphase separation and ordering. On the other hand, if the vapor pressure is too low (Fig. 4a), the chain mobility may not be enough to reach an equilibrium state during solvent annealing. The best ordering was acquired for

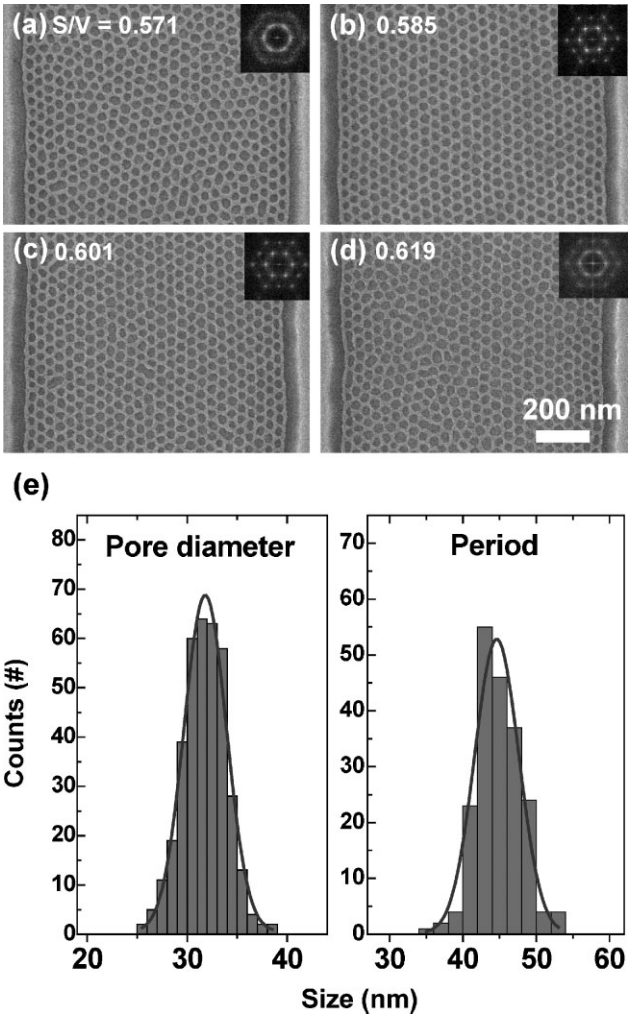

Figure 4. a–d) SEM images of perforated lamellar morphologies annealed at various vapor pressures. The S/V ratios are 0.571 (a), 0.585 (b), 0.601 (c), and 0.619 (d) cm^{-1}. The insets show fast Fourier transforms. The best ordering obtained was at $S/V = 0.585$ and $0.601\,cm^{-1}$. e) Histograms of pore diameters (31.7 ± 2.1 nm) and average center-to-center spacing (44.8 ± 3.1 nm) of the pores for the morphology in (b).

the intermediate vapor pressure conditions ($S/V = 0.585$, $0.601\,cm^{-1}$), but a small number of local defects was still present. The most common defect was the lack of bridges between neighboring pores.

A large well-ordered perforated lamellar area produced at $S/V = 0.585\,cm^{-1}$ (Fig. 4b and S2c, see Supporting Information) had an average center-to-center spacing of 44.8 ± 3.1 nm and a pore diameter of 31.7 ± 2.1 nm. The size distribution of the spacing and pore diameter are provided as histograms in Figure 4e. The pores were arranged with their close-packed direction parallel to the trench walls; this orientation is analogous to an arrangement of hexagonally ordered spherical BCP domains in one-dimensional trenches.[40]

Nanoporous patterns, which are useful for making hole arrays by etching or dots by a lift-off process, are usually produced by orienting cylindrical BCP domains perpendicularly to a substrate with neutral interfaces and then selectively removing the cylinders.[2,41] The formation of templated nanoporous patterns in PS–PDMS using mixed solvent annealing is significant because it is difficult to obtain a pore array from a perpendicular cylinder morphology, due to the very large surface energy difference between the two blocks. The nanoporous PDMS structures described here will be particularly useful in making hole arrays, due to their high etch resistance.

In summary, we have shown how the geometry of thin films of a cylinder-forming BCP can be tuned to a wide range of morphologies by using controlled solvent vapors. Control of two solvent-annealing parameters, the solvent mixing ratio and the vapor pressure, affect the period length of parallel cylinder arrays and the linewidth of individual cylinders. This control can also lead to different morphologies, such as a perforated lamellar structure. The demonstration of independent control over the linewidth and the period length is useful for BCP-based fabrication of device structures. This process may also be applicable to other morphologies, such as spheres, and to other material systems, such as micelles or organic-surfactant-coated nanoparticles.

Experimental

Si substrates patterned with 40 nm deep trenches with a periodicity of 1.3 μm were fabricated using a Lloyd's Mirror interference lithography system with a He–Cd laser operating at 325 nm. The laser exposed grating patterns into PFI-88 photoresist with a thickness of 200 nm (Sumitomo Chemical Co., Japan), which were transferred onto the Si substrate by CF_4 reactive-ion etching at 10 mTorr (1 Torr = 133.32 Pa). The native oxide surfaces were treated with a hydroxy-terminated PDMS homopolymer (molecular weight: $5\,kg\,mol^{-1}$, Polymer Source, Inc., Canada), which was spun-cast onto the substrates and annealed at 150 °C for 15 h. The surfaces were then washed with toluene to remove any unattached polymers. The thickness of the grafted brush layer was estimated to be around 3–4 nm by ellipsometry. Thin films of a cylinder-forming PS-PDMS block copolymer (Polymer Source, Inc., Canada) with a total molecular weight of $45.5\,kg\,mol^{-1}$ and a nominal volume fraction of PDMS (f_{DMS}) of 33.5% were then spin-coated onto the substrates. Films with a thickness of 30 nm were produced by spin-casting toluene solutions of the BCP (1.5 wt%). The samples were then solvent-annealed under toluene or toluene–heptane vapor at room temperature for 3 h. Solvent vapor pressure was controlled via the ratio between the surface area of the liquid solvent and the empty volume of the annealing chamber [11]. The annealed films were treated with CF_4 plasma (50 W, 5 s) followed by O_2 plasma (90 W, 22 s) to remove the PDMS surface layer and to selectively eliminate the PS block, resulting in oxidized PDMS microdomains within the substrate trenches.

Surface morphology was observed using a Zeiss/Leo Gemini 982 SEM operated with an acceleration voltage of 5 kV. A thin layer of Au–Pd alloy was sputter-coated onto the samples in order to avoid charging effects.

Acknowledgements

The authors thank the Semiconductor Research Corporation for financial support. Supporting Information is available online from Wiley InterScience or from the author.

Received: September 26, 2008
Published online: April 8, 2009

[1] M. Park, C. Harrison, P. M. Chaikin, R. A. Register, D. H. Adamson, *Science* **1997**, *276*, 1401.
[2] T. Thurn-Albrecht, J. Schotter, C. A. Kastle, N. Emley, T. Shibauchi, L. Krusin-Elbaum, K. Guarini, C. T. Black, M. T. Tuominen, T. P. Russell, *Science* **2000**, *290*, 2126.
[3] J. Y. Cheng, C. A. Ross, E. L. Thomas, H. I. Smith, G. J. Vancso, *Adv. Mater.* **2003**, *15*, 1599.
[4] S. O. Kim, H. H. Solak, M. P. Stoykovich, N. J. Ferrier, J. J. de Pablo, P. F. Nealey, *Nature* **2003**, *424*, 411.
[5] R. A. Segalman, A. Hexemer, E. J. Kramer, *Phys. Rev. Lett.* **2003**, *91*, 196101.
[6] C. T. Black, O. Bezencenet, *IEEE Trans. Nanotechnol.* **2004**, *3*, 412.
[7] D. Sundrani, S. B. Darling, S. J. Sibener, *Nano Lett.* **2004**, *4*, 273.
[8] C. T. Black, *Appl. Phys. Lett.* **2005**, *87*, 163116.
[9] C. T. Black, R. Ruiz, G. Breyta, J. Y. Cheng, M. E. Colburn, K. W. Guarini, H. C. Kim, Y. Zhang, *IBM J. Res. Dev.* **2007**, *51*, 605.
[10] S. B. Darling, *Prog. Poly. Sci.* **2007**, *32*, 1152.
[11] Y. S. Jung, C. A. Ross, *Nano Lett.* **2007**, *7*, 2046.
[12] L. Rockford, S. G. J. Mochrie, T. P. Russell, *Macromolecules* **2001**, *34*, 1487.
[13] R. Ruiz, H. M. Kang, F. A. Detcheverry, E. Dobisz, D. S. Kercher, T. R. Albrecht, J. J. de Pablo, P. F. Nealey, *Science* **2008**, *321*, 936.
[14] Y. Y. Wu, G. S. Cheng, K. Katsov, S. W. Sides, J. F. Wang, J. Tang, G. H. Fredrickson, M. Moskovits, G. D. Stucky, *Nat. Mater.* **2004**, *3*, 816.
[15] H. Q. Xiang, K. Shin, T. Kim, S. I. Moon, T. J. McCarthy, T. P. Russell, *Macromolecules* **2004**, *37*, 5660.
[16] Y. S. Jung, W. Jung, C. A. Ross, *Nano Lett.* **2008**, *8*, 2975.
[17] F. S. Bates, G. H. Fredrickson, *Annu. Rev. Phys. Chem.* **1990**, *41*, 525.
[18] E. Helfand, Y. Tagami, *J. Chem. Phys.* **1972**, *56*, 3592.
[19] M. P. Stoykovich, M. Muller, S. O. Kim, H. H. Solak, E. W. Edwards, J. J. de Pablo, P. F. Nealey, *Science* **2005**, *308*, 1442.
[20] G. Kim, M. Libera, *Macromolecules* **1998**, *31*, 2569.
[21] K. Fukunaga, H. Elbs, R. Magerle, G. Krausch, *Macromolecules* **2000**, *33*, 947.
[22] S. H. Kim, M. J. Misner, T. P. Russell, *Adv. Mater.* **2004**, *16*, 2119.
[23] J. Peng, Y. Xuan, H. F. Wang, Y. M. Yang, B. Y. Li, Y. C. Han, *J. Chem. Phys.* **2004**, *120*, 11163.
[24] K. A. Cavicchi, K. J. Berthiaume, T. P. Russell, *Polymer* **2005**, *46*, 11635.
[25] J. Bang, S. H. Kim, E. Drockenmuller, M. J. Misner, T. P. Russell, C. J. Hawker, *J. Am. Chem. Soc.* **2006**, *128*, 7622.
[26] J. K. Bosworth, M. Y. Paik, R. Ruiz, E. L. Schwartz, J. Q. Huang, A. W. Ko, D. M. Smilgies, C. T. Black, C. K. Ober, *ACS Nano* **2008**, *2*, 1396.
[27] J. Bang, B. J. Kim, G. E. Stein, T. P. Russell, X. Li, J. Wang, E. J. Kramer, C. J. Hawker, *Macromolecules* **2007**, *40*, 7019.

[28] R. Guo, H. Y. Huang, Y. Z. Chen, Y. M. Gong, B. Y. Du, T. B. He, *Macromolecules* **2008**, *41*, 890.
[29] I. Bita, J. K. W. Yang, Y. S. Jung, C. A. Ross, E. L. Thomas, K. K. Berggren, *Science* **2008**, *321*, 939.
[30] A. Knoll, A. Horvat, K. S. Lyakhova, G. Krausch, G. J. A. Sevink, A. V. Zvelindovsky, R. Magerle, *Phys. Rev. Lett.* **2002**, *89*, 035501.
[31] T. Hashimoto, M. Shibayama, H. Kawai, *Macromolecules* **1983**, *16*, 1093.
[32] S. Alexander, *J. Phys. (Paris)* **1977**, *38*, 977.
[33] P. G. Degennes, *Macromolecules* **1980**, *13*, 1069.
[34] S. P. Gido, E. L. Thomas, *Macromolecules* **1997**, *30*, 3739.
[35] E. Helfand, Z. R. Wasserman, *Macromolecules* **1980**, *13*, 994.
[36] S. P. Gido, D. W. Schwark, E. L. Thomas, M. D. Goncalves, *Macromolecules* **1993**, *26*, 2636.
[37] A. F. Barton, *CRC Handbook of Solubility Parameters and Other Cohesion Parameters*, CRC Press, Boca Raton, FL **1991**.
[38] S. Ludwigs, A. Boker, A. Voronov, N. Rehse, R. Magerle, G. Krausch, *Nat. Mater.* **2003**, *2*, 744.
[39] I. Park, S. Park, H. W. Park, T. Chang, H. C. Yang, C. Y. Ryu, *Macromolecules* **2006**, *39*, 315.
[40] R. A. Segalman, H. Yokoyama, E. J. Kramer, *Adv. Mater.* **2001**, *13*, 1152.
[41] D. Y. Ryu, K. Shin, E. Drockenmuller, C. J. Hawker, T. P. Russell, *Science* **2005**, *308*, 236.